molecules

MDPI

Article

Pyridinium Salts of Dehydrated Lanthanide Polychlorides

Roger E. Cramer [1], Esteban M. Baca [2] and Timothy J. Boyle [2,*]

[1] Department of Chemistry, University of Hawaii—Manoa, 2545 McCarthy Mall, Honolulu, HI 96822, USA
[2] Advanced Materials Laboratory, Sandia National Laboratories, 1001 University Boulevard, SE, Albuquerque, NM 87106, USA
* Correspondence: tjboyle@sandia.gov; Tel.: +1-(505)-272-7625

Abstract: The reaction of lanthanide (Ln) chloride hydrates ($[Ln(H_2O)_n(Cl)_3]$) with pyridine (py) yielded a set of dehydrated pyridinium (py-H) Ln-polychloride salts. These species were crystallographically characterized as $[[py\text{-}H\text{-}py][py\text{-}H]_2[LnCl_6]]$ (**Ln-6**; Ln = La, Ce, Pr, Nd, Sm, Eu, Gd) or $[[py\text{-}H]_2[LnCl_5(py)]]$ ((**Ln-5**; Ln = Tb, Dy, Ho, Er, Tm, Yb, Lu). The **Ln-6** metal centers adopt an octahedral (*OC*-6) geometry, binding six Cl ligands. The −3 charge is off-set by two py-H moieties and a di-pyridinium (py-H-py) ion. For the **Ln-5** species, an *OC*-6 anion is formed by the Ln cation binding a single py and five Cl ligands. The remaining −2 charge is offset by two py-H^+ cations that H-bond to the anion. Significant H-bonding occurs between the various cation/anion moieties inducing the molecular stability. The change in structure from the **Ln-6** to **Ln-5** is believed to be due to the Ln-contraction producing a smaller unit cell, which prevents formation of the py-H-py^+ cation, leading to the loss of the H-bonding-induced stability. Based on this, it was determined that the **Ln-5** structures only exist when the lattice energy is small. While dehydrated polychloride salts can be produced by simply mixing in pyridine, the final structures adopted result from a delicate balance of cation size, Coulombic charge, and stabilizing H-bonding.

Keywords: lanthanides; chlorides; hydrate; dehydration; pyridinium

Citation: Cramer, R.E.; Baca, E.M.; Boyle, T.J. Pyridinium Salts of Dehydrated Lanthanide Polychlorides. *Molecules* **2023**, *28*, 283. https://doi.org/10.3390/molecules28010283

Academic Editor: Barbara Modec

Received: 4 November 2022
Revised: 7 December 2022
Accepted: 20 December 2022
Published: 29 December 2022

1. Introduction

Lanthanide-based materials have found widespread use in numerous everyday applications such as electronic, automobile, audio, and battery purposes. These critical materials are typically isolated from monazite ores using complicated ion exchange processes that generate large amounts of waste and involve extensive labor and energy input to obtain pure materials [1–3]. Recycling efforts pertaining to the Ln cations have come to the forefront as a means to recover and reuse the already separated Ln-element. Recycling usually involves the dissolution of the Ln in a strong acid (HNO_3, H_2SO_4 [4], or HX [5] (X = Cl, Br, I)). One product isolated from the reaction of Ln-based materials (Ln(0) or Ln_2O_3) using hydrochloric acid (HCl) are the Ln, chloro, hydrates that form either $[Ln(m\text{-}Cl)(H_2O)_7]_2\bullet 4Cl$ (Ln = La, Ce, Pr) or $[LnCl_2(H_2O)_6]\bullet Cl$ (Ln = Nd to Lu) [3], often erroneously, referred to as $LnCl_3\bullet 6H_2O$ for simplicity. For this effort, this family of precursors are referred to as $[Ln(H_2O)_n(Cl)_3]$. Lanthanide halides (LnX_3) are ubiquitous starting materials for synthetic efforts since the ease of halide metathesis affords the facile production of other synthons [3]. However, for these reactions it is critically important to utilize anhydrous materials to prevent detrimental side-reactions. Hence, methods to dehydrate the $[Ln(H_2O)_n(Cl)_3]$ precursors is necessary. Typically, this is achieved from the reaction of the starting material with NH_4Cl to form the ammonium pentachloride Ln-derivative ($[(NH_4)_2LnCl_5]$), followed by heat and sublimation to remove NH_3 and HCl [6].

Previously, we found that the Sc-chloro-hydrate could be easily dehydrated merely by dissolving the hydrate in an appropriate solvent [7]. Due to this success, a similar simple dissolution/solvation approach to displace the bound H_2O was undertaken using $[Ln(H_2O)_n(Cl)_3]$ and a wide range of solvents. Of these studies, the pyridine dissolution

products proved to be anhydrous, forming polychloro, pyridinium (py-H) products (eq 1). The products were identified by crystallographic studies as either [[py-H-py][py-H]$_2$[LnCl$_6$]] (**Ln-6**; Ln = La to Gd) or [[py-H]$_2$[LnCl$_5$(py)]] ((**Ln-5**; Ln = Tb to Lu). Details of the synthesis and final structures isolated are presented.

$$\mathbf{[Ln(H_2O)_{\mathit{n}}(Cl)_3] + (xs)\ py \rightarrow [z[py\text{-}H\text{-}py][Py\text{-}H]_2[LnX_x(py)_y]]} \quad (1)$$

$x = 6, y = 0, z = 1$: *Ln* = ($n = 7$) *La*, *Ce*, *Pr*, ($n = 6$) *Nd*, *Sm*, *Eu*, *Gd*

$x = 5, y = 1, z = 0, n = 6$: *Ln* = *Tb*, *Dy*, *Ho*, *Er*, *Tm*, *Yb*, *Lu*

2. Results and Discussion

Searching for solvents that could easily dehydrate **[Ln(H$_2$O)$_n$(Cl)$_3$]** led to the exploration of pyridine. This selection was based on the ready formation of NH_3 products during NH_4Cl dehydration processing indicating the facile displacement of water by amines and the unusual structures noted below using pyridine.

A number of Ln-polychloride py-H salts have been reported, including [py-H]$_2$[CeCl$_6$], [py-H]$_2$[LnCl$_5$(py)] (where Ln = Eu, Er, Yb) [8]or [py-H][YbCl$_4$(py)$_2$]•py [8]. Information pertaining to the reported Ce(IV) hexachloride is limited as there are no coordinates supplied and the early issues of the journal are not readily available. The previously reported pentachlorides were prepared by heating the anhydrous $LnCl_3$ in diacetone alcohol (DAA) and pyridine for 9 h at 100 °C. The products are octahedrally (*OC*-6) bound Ln cations with 5 inner-sphere Cl and a bound py. The 2-charge is balanced by two lattice H-py cations. The long-range order of the crystal results from H-bonding between Cl atoms and the nearest neighbors H-py. For this report, a study of the products from the simple reaction of **[Ln(H$_2$O)$_n$(Cl)$_3$]** heated in a solution of py was undertaken.

2.1. Synthesis

Initial efforts focused on the [Ce(m-Cl)(H$_2$O)$_7$]$_2$•4Cl precursor. The sample was slurried in pyridine, centrifuged and the soluble fraction allowed to slowly evaporate. From this 'wash', a mixed ligand complex was isolated as [py-H]$_2$[Ce(Cl)$_2$(H$_2$O)$_6$][Cl]$_3$(H$_2$O) (**Ce-H$_2$O/py-H**). Figure 1 shows the structure of **Ce-H$_2$O/py-H**. This unusual eight-coordinated monomeric complex reveals that one of the Cl ions moved from the outer-sphere to the inner-sphere while three other Cl atoms remained in the outer-sphere and are charge balanced by py-H moieties. These changes, reduce the dinuclear starting material to a monomer. This is believed to be the first step in the dehydration that was observed below. The quality of the crystal structure solution of **Ce-H$_2$O/py-H** is high enough to verify connectivity but not sufficient for publication due to low data parameter ratio but is included here (see Table 1) for completeness. Interestingly, **Ce-H$_2$O/py-H** does not show any loss of water; thus, additional studies were undertaken to induce dehydration.

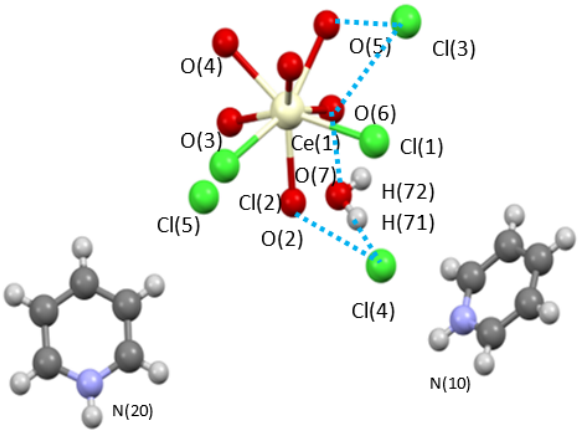

Figure 1. Ball and stick structure plot of [Ce(Cl)$_2$(OH$_2$)$_6$][py-H]$_2$[Cl]$_3$(H$_2$O) (**Ce-H$_2$O/py-H**). Blue dashed line represents H-bonding.

Table 1. Data collection parameters for **La-6 to Ce-H_2O**.

Compound	**La-6**	**Ce-6**	**Pr-6**
Chem. Form	$C_{20}H_{23}Cl_6N_4La$	$C_{20}H_{23}CeCl_6N_4$	$C_{20}H_{23}Cl_6N_4Pr$
Form. weight	335.02	672.24	673.03
temp (K)	100 (2)	100 (2)	100 (2)
space group	Orthorhombic P 2_1 2_1 2_1	Orthorhombic P 2_1 2_1 2_1	Monoclinic $P2_1/c$
a (Å)	9.7104(6)	9.6382(3)	15.6181(11)
b (Å)	15.6614(10	15.6027(4)	9.5868(8)
c (Å)	18.1015(12)	18.0596(6)	36.244(3)
b (deg)			89.999(3)
V (Å^3)	2752.8(3)	2715.84(14)	5426.8(7)
Z	4	4	8
D_{calcd} (Mg/m^3)	1.619	1.644	1.648
m (Mo, Ka) (mm^{-1})	2.149	2.282	2.402
Flack Parameter	0.500(6)	0.50(1)	NA [c]
R1 [a] (%) (all data)	2.25 (2.65)	2.22 (2.22)	5.55 (10.16)
wR2 [b] (%) (all data)	4.86 (5.18)	6.14 (6.15)	10.15 (12.71)
Compound	**Nd-6**	**Sm-6**	**Eu-6**
Chem. Form	$C_{20}H_{23}Cl_6N_4Nd$	$C_{20}H_{23}Cl_6N_4Sm$	$C_{20}H_{23}Cl_6EuN_4$
Form. weight	676.36	682.47	684.08
temp (K)	100 (2)	100 (2)	100 (2)
space group	Monoclinic $P2_1/c$	Monoclinic $P2_1/c$	Monoclinic $P2_1/c$
a (Å)	15.561(2)	15.5230(14)	15.534(3)
b (Å)	9.5667(15)	9.5386(9)	9.5290(19)
c (Å)	36.204(5)	36.265(4)	36.287(7)
b (deg)	90.306(5)	90.244(4)	90.091(7)
V (Å^3)	5389.3(14)	5369.6(9)	5371.5(18)
Z	8	8	8
D_{calcd}(Mg/m^3)	1.667	1.688	1.692
m (Mo, Ka) (mm^{-1})	2.537	2.800	2.948
Flack Parameter	NA	NA	NA
R1 [a] (%) (all data)	8.14 (13.45)	4.45 (6.04)	4.81 (9.68)
wR2 [b] (%) (all data)	16.45 (19.59)	9.48 (10.78)	11.22 (15.11)
Compound	**Gd-6**	**Tb-5**	**Dy-5**
Chem. Form	$C_{20}H_{23}Cl_6GdN_4$	$C_{15}H_{17}Cl_5N_3Tb$	$C_{15}H_{17}Cl_5DyN_3$
Form. weight	689.37	572.48	579.06
temp (K)	100 (2)	100 (2)	100(2)
space group	Monoclinic $P2_1/c$	Orthorhombic $Pna2_1$	Orthorhombic $Pna2_1$
a (Å)	15.5351(13)	15.561(2)	18.693(3)
b (Å)	9.5079(8)	9.5667(15)	7.3078(10)
c (Å)	36.279(3)	36.204(5)	14.789(2)
b (deg)	90.055(3)		

Table 1. *Cont.*

V (Å^3)	5358.6(8)	2028.3(3)	2020.3(5)
Z	8	4	4
D_{calcd}(Mg/m^3)	1.709	1.885	1.904
m (Mo, Ka) (mm^{-1})	3.089	4.148	4.362
Flack Parameter	NA	0.500(9)	0.459(6)
R1 [a] (%) (all data)	6.38 (7.36)	1.78 (1.98)	1.37 (1.40)
wR2 [b] (%) (all data)	13.85 (14.77)	3.65 (3.71)	3.25 (3.30)
Compound	**Ho-5**	**Er-5**	**Tm-5**
Chem. Form	$C_{15}H_{17}Cl_5HoN_3$	$C_{15}H_{17}Cl_5ErN_3$	$C_{15}H_{17}Cl_5N_3Tm$
Form. weight	581.49	583.82	585.49
temp (K)	100 (2)	100 (2)	100 (2)
space group	Orthorhombic $Pna2_1$	Orthorhombic $Pna2_1$	Orthorhombic $Pna2_1$
a (Å)	18.6738(17)	18.6315(7)	18.6333(11)
b (Å)	7.2976(6)	7.2898(3)	7.2815(4)
c (Å)	14.7913(13)	14.7705(5)	14.7648(9)
V (Å^3)	2015.7(3)	2006.13(13)	2003.3(2)
Z	4	4	4
D_{calcd}(Mg/m^3)	1.916	1.933	1.941
m (Mo, Ka) (mm^{-1})	4.590	4.852	5.098
Flack Parameter	0.465(5)	0.486(5)	0.350(8)
R1 [a] (%) (all data)	1.65 (1.71)	1.05 (1.06)	2.27 (2.76)
wR2 [b] (%) (all data)	3.78 (3.79)	2.67 (2.68)	4.92 (5.28)
Compound	**Yb-5**	**Lu-5**	**Ce-H_2O/py-H**
Chem. Form	$C_{15}H_{17}Cl_5N_3Yb$	$C_{15}H_{17}Cl_5N_3Lu$	$C_{10}H_{26}CeCl_5N_2O_7$
Form. weight	589.60	591.54	603.70
temp (K)	100 (2)	100 (2)	100(2)
space group	Orthorhombic $Pna2_1$	Orthorhombic $Pna2_1$	Monoclinic $P2_1/n$
a (Å)	18.6135(11)	18.8935(3)	8.4460(8)
b (Å)	7.2804(4)	7.27030(10)	17.5550(18)
c (Å)	147520(9))	14.7377(3)	15.5427(18)
b(deg)			91.534(3)
V (Å^3)	1999.1(2)	1992.25(6)	2303.7(4)
Z	4	4	4
D_{calcd}(Mg/m^3)	1.959	1.972	1.741
m (Mo, Ka) (mm^{-1})	5.349	5.628	2.585
Flack Parameter	0.457(7)	0.488(6)	
R1 [a] (%) (all data)	2.16 (2.45)	1.90 (2.73)	5.50 (5.73)
wR2 [b] (%) (all data)	4.63 (4.81)	3.41 (3.56)	18.67 (18.84)

[a] $\mathbf{R1 = \Sigma \mid \mid F_o \mid - \mid F_c \mid \mid / S \mid F_o \mid \times 100}$; [b] $\mathbf{wR2 = [\Sigma\, w\,(F_o^2 - F_c^2)^2 / \Sigma\,(w \mid F_o \mid^2)^2]^{1/2} \times 100}$; [c] NA = **Not applicable.**

Further studies using the early, lighter **[Ln(H_2O)$_n$(Cl)$_3$]** precursors were initiated and various **[Ln(H_2O)$_n$(Cl)$_3$]** were stirred in pyridine overnight (12 h). Instead of a clear

solution a white slurry formed. In order to induce maximum substitution, the mixture was heated to a boil, and while hot, the mixture was poured through a glass frit. The clear mother liquor was allowed to sit, yielding crystals in all instances. Based on the isolation, the formation of pyridinium ions was expected with a change in inner and outer-sphere Cl ions but the extent of dehydration was surprising.

2.2. Characterization

FTIR data were collected since the Ln-Cl interaction would not complicate the spectrum and the presence of either water or pyridine could be readily observed. The FTIR spectral data for all of the compounds reported are available in the Supporting Information (see Figures S1–S14). The loss of the broad -OH stretch around 3000 cm^{-1} for all of the compounds indicated the products were successfully dehydrated. There were also stretches present above 2461 cm^{-1} consistent with a N-H moiety. These would include the five stretches around 1633, 1599, 1531, 1487, and 1445 cm^{-1} that were previously associated with the nuclear variations consistent with displacement of the pyridine ring. Additionally, the 767 and 700 cm^{-1} stretches observed in the spectra are associated with the C-H and C-C bends of the pyridine rings. There is an additional stretch located around 600 cm^{-1} for the light Ln (La to Gd) and then a shift to 623 cm^{-1} for the heavy Ln (Tb-Lu), which may represent the La-Cl interaction. These assignments are consistent with the py-H salts of other metal halides presented by Cook [9].

2.2.1. Crystal Structures

As the remainder of analytical inspections proved fruitless due to the paramagnetic nature of the cations, the presence of halide ligands, and the inconsistencies (volatility, additional trapped or premature loss) of solvated species, crystal structure determination was primarily used to identify the structures of the final products. With the isolation of the crystal structures (*vide infra)*, powder XRD analyses on each powder was undertaken and compared with the calculated patterns. These are shown in the Supporting Information. In general, the bulk powder experimental patters for **Ln-6** and **Ln-5** samples appear to be in agreement with the larger peaks associated with the calculated patterns; however, the substantial other peaks present indicate potential other products and organic species may be present in the final products. It is of note, that numerous crystals were studied for each cation with a consistent isolation of either the **Ln-6** or **Ln-5** observed for each sample.

Three structures and two compositions were observed in this study: [[py-H-py][py-H]$_2$[$LnCl_6$]] (**Ln-6**: Ln = La and Ce—crystallize in the orthorhombic space group $P2_12_12_1$; **Ln** = Pr, Nd, Sm, Eu, and Gd—crystallize in the monoclinic space group $P2_1/c$) and [[py-H]$_2$[$LnCl_5$(py)]] (**Ln-5**; Ln = Tb, Dy, Ho, Er, Tm, Yb, and Lu—crystallize in the orthorhombic space group $Pna2_1$). Figures 2 and 3 show the representative structure plots of the **Ln-6** [[py-H-py][py-H]$_2$[$EuCl_6$]] (**Eu-6**) and the **Ln-5** [[py-H]$_2$[$LuCl_5$(py)]] (**Lu-5**) structures observed in this work. Table 1 lists the data collection parameters for all compounds. Tables 2 and 3 list the average metrical data for the **Ln-6** and **Ln-5** compounds, respectively.

Since any changes in structural properties within the Ln series are expected to be very small due to the Ln-contraction, the three structure types are also expected to have very similar stabilities. In each case (i.e., **Ln-6** and **Ln-5**) an octahedral $LnCl_6$ or $LnCl_5$(py) polyanion is surrounded by a shell of py-H and/or py-H-py cations. The py-H cations H-bond to Cl ligands coupled with extensive C-H●●●Cl H-bonding, which holds the lattice together for crystal formation. These interactions are shown in the packing diagrams for **Ln-6** and **Ln-5** (Figures 1 and 2b, respectively). For the **Ln-6** species, the compounds are distorted from an ideal *OC*-6 geometry by H-bonds formed between the Cl ligands and the H-py cations. The *trans*-Cl angles range from 168.1 to 178.6°, with an average of 176.6°; however, the *trans*-Cl atoms that are independently bound to a H-py, are at the low end of this range. The N_{py}-H●●●Cl angles range from 152.1 to 175.6° (av 165.1°). For the **Ln-5**, a distorted *OC*-6 geometry results from the binding of five Cl and one py ligand. The *trans* Cl angles span the relatively small range of 174.9 to 177.6° (av. 176.6); the *trans* Cl---N av

177.3 from a range of 177.1 to 178.0°. The N_{py}-H---Cl av 177.4° with a range of 177.1 to 178.0°. The average Ln-Cl distances for **Ln-6** (av 2.73 Å) are slightly longer than that of **Ln-5** (av 2.61 Å) compounds. This also results in longer Cl---Cl distances for **Ln-6** vs. **Ln-5** (av) 3.85 vs. 3.69 Å, respectively. The Ln-N distance for **Ln-5** (av 2.49 Å) are in agreement with literature values [10]. However, it is not readily apparent why the structure changes from **Ln-6** to **Ln-5** based on the metrical data alone.

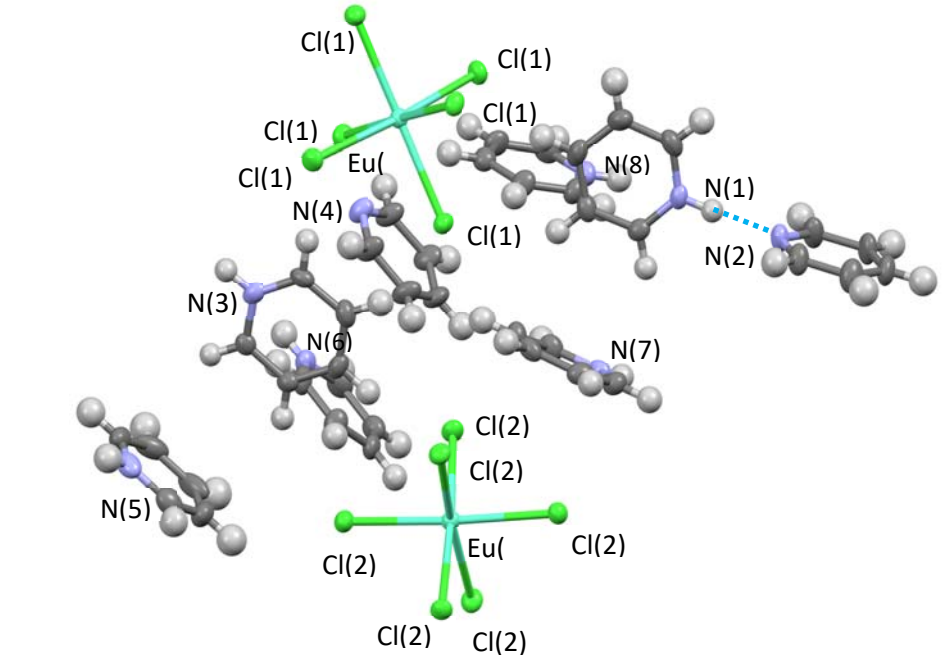

(**a**)

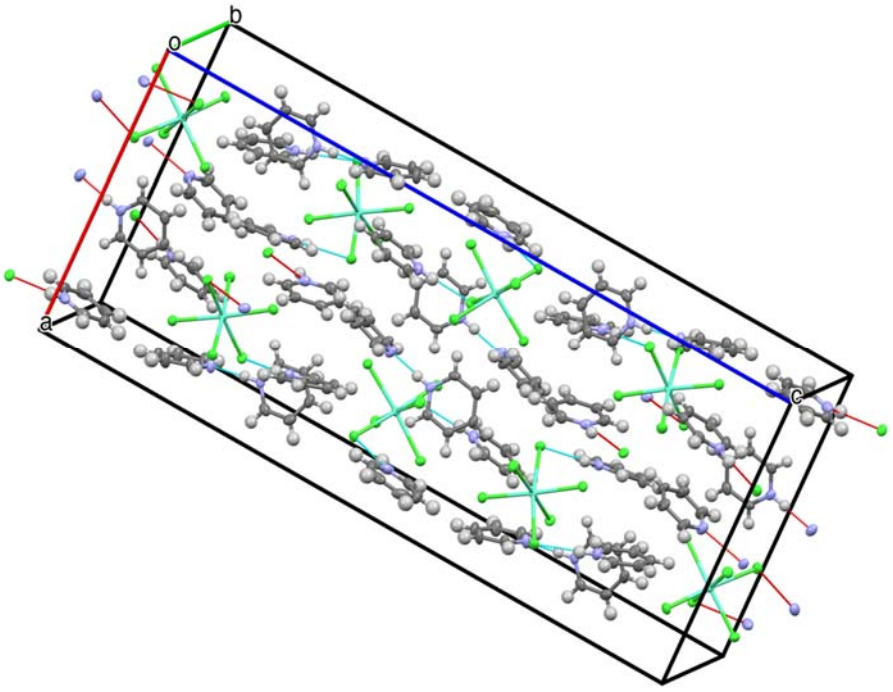

(**b**)

Figure 2. Structure plot of [[py-H-py][py-H]$_2$[$EuCl_6$]] (**Eu-6**) (**a**) unit cell solution and (**b**) packing diagram with H-bonding shown in blue dashes and short contacts in red. Thermal ellipsoids are drawn at 50% level.

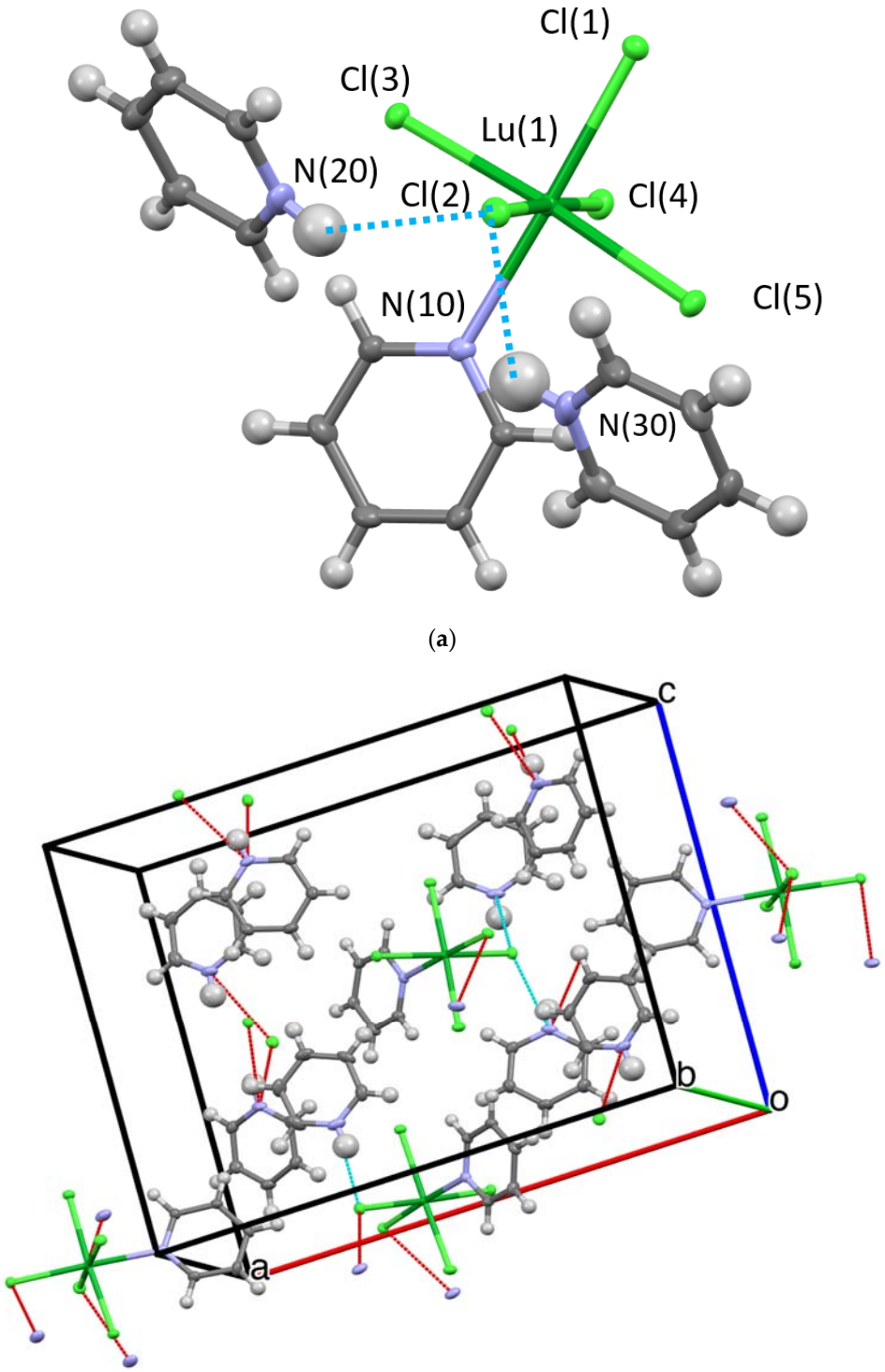

Figure 3. Structure plot of $[[py\text{-}H]_2[LuCl_5(py)]]$ (**Lu-5**): ((**a**) unit cell solution and (**b**) packing diagram with H-bonding shown in blue dashes and short contacts in red. Thermal ellipsoids are drawn at 50% level. Blue dashed line represents H-bonding and red lines, short contacts.

Table 2. Average, select, metrical data for **Ln-6**.

Distance (Å)	**La**	**Ce**	**Pr**	**Nd**	**Sm**	**Eu**	**Gd**
Ln-Cl	2.796	2.758	2.737	2.724	2.702	2.689	2.676
Cl---Cl	3.954	3.900	3.871	3.852	3.821	3.803	3.784
(py)N-H-N(py)	2.678	2.678	2.672	2.674	2.664	2.678	2.676
(py)N-H---Cl	3.165	3.171	3.210	3.179	3.164	3.171	3.181
Angles (deg)	**La**	**Ce**	**Pr**	**Nd**	**Sm**	**Eu**	**Gd**
trans Cl-Ln-Cl	173.11	172.18	174.43	175.00	174.48	173.45	174.43
(py)N-H-N(py)	171.80	170.96	174.11	174.20	173.58	173.97	171.91
(py)N-H---Cl	169.63	168.77	164.87	165.67	165.67	164.88	164.47

Table 3. Average, select, metrical data for **Ln-5**.

Distance (Å)	**Tb**	**Dy**	**Ho**	**Er**	**Tm**	**Yb**	**Lu**
Ln-Cl	2.643	2.638	2.633	2.602	2.597	2.591	2.576
Cl---Cl	3.738	3.73	3.726	3.680	3.673	3.664	3.643
Ln-N(py)	2.524	2.517	2.507	2.507	2.475	2.475	2.454
(py)N-H---Cl	3.230	3.232	3.229	3.276	3.235	3.274	3.265
Angles (deg)	**Tb**	**Dy**	**Ho**	**Er**	**Tm**	**Yb**	**Lu**
trans Cl-Ln-Cl	176.105	176.37	176.37	176.615	176.71	176.805	176.775
tans Cl-Ln-N(py)	177.19	177.28	177.29	177.11	177.47	178.06	177.36
(py)N-H---Cl	177.19	177.28	177.29	177.11	177.47	178.06	177.36

The lanthanides are often claimed to have uniform chemistry, with the assumption that one structure represents the entire series. This is often based on lore or the small handful of examples where the entire series has been studied [11]. As noted for this series, the structure changes from **Gd-6** to **Tb-5**, which can only occur if the overall energies of the two structures are very similar. Therefore, the differences in these two structures must come from: Hydrogen Bonding, Bonding Energy, and Lattice Energy. An exploration of these variables is discussed below along with a Crystal Stress Analysis and Stress Summary in an attempt to explain why this unusual structural change occurs.

Hydrogen Bonding

In all three structure types, the two py-H cations H-bond to Cl ligands with average N-H●●●Cl distances tabulated in Table 2. From these data, it is apparent that these distances are slightly shorter for the **Ln-6** (av 3.18 Å) in comparison to the **Ln-5** (av 3.25 Å) structures. Thus, the H-bonding of the py-H cations to Cl ligands is favored in the **Ln-6** structure by ~5 Kcal/mole [12]. Furthermore, in both structures, nearly every C-H bond of the pyridine rings forms a C-H●●●Cl H-bond (see Tables S4 and S5). In the **Ln-6** structures, the two py-H cations form 13 H-bonds while in the **Ln-5** structure only 11 were observed. Thus, H-bonding is favored in the **Ln-6** structures, but by only by a slight amount since the C-H●●●Cl hydrogen bonds are quite weak. In addition, the **Ln-6** structure contains a py-H-py cation. As can be seen in Table 2, this cation contains one very short and strong H-bond estimated to be ~10 Kcal/mole. In addition, each py-H-py cation forms eight or nine C-H●●●Cl H-bonds, which is estimated to add another 10 Kcal/mole stabilization to the **Ln-6** structure. Summation of these values (see Table S6) favors the **Ln-6** structure by ~25 Kcal/mole. The Cambridge Structural Database lists 125 structures with a $LnCl_6$ anion [10] with 123 of these using either an ammonium, phosphonium, or protonated aromatic amine cations. Moreover, all these feature extensive H-bonding between the $LnCl_6$

anions and the various cations, often involving C-H●●●Cl H-bonds. This is consistent with the **Ln-6** structures reported in this work.

Bonding Energy

The covalency of the bonds for $LnCl_6$ anions was previously investigated both experimentally and theoretically [13]. From this study, it was determined that the degree of covalent nature was between 3% and 12%. Since this contribution is so small, full ionic character was assumed and binding energies were calculated using Coulombs Law (see Table S6 for final values). For this evaluation, three energy terms were considered: (i) the Ln-Cl attraction, (ii) *cis* Cl---Cl repulsion, and (iii) *trans* Cl---Cl repulsion. Even though the Ln-Cl attraction is greater than the *cis* Cl---Cl repulsion, it was found that the **Ln-6** anion is inherently unstable when the *trans* Cl---Cl repulsion is included. In contrast, the **Ln-5** anion has less Cl---Cl repulsion due to the presence of the py ligand and is more stable than the **Ln-6** structure by a substantial amount.

If a covalent contribution is considered, the negative charge on the Cl ligands would be reduced, producing a weaker Ln-Cl attraction. This change is offset (wholly or partially) by the covalent contribution to the bond. The reduced Cl negative charge also reduces the Cl---Cl repulsions. Using an average 5% covalent contribution [13], the unfavorable $GdCl_6^{-3}$ anion's energy is reduced to ~90 kcal/mol. In comparison, the $LnCl_5^{-2}$ becomes even more stable, as the Cl---Cl repulsion is reduced. These calculations ignore the distance controlled, ion–dipole Ln-py interaction. The Ln-N_{py} is significantly shorter than the *cis* or *trans* Cl---N distances, suggesting this has greater influence on the final stability than any Cl---N repulsion. Thus, it is assumed the Ln-N_{py} will only add to the stability of the final anion for the **Ln-5** complexes. This raises the question as to why the early Ln cations did not form the same structure. Therefore, the **Ln-6** compositions must possess a significant contribution from another source in order to generate a stable structure.

Lattice Energy

The final factor in the overall stability of the **Ln-6** and **Ln-5** structures would be the lattice energy. Lattice energy (U) can be written as (Equation (2)):

$$\mathbf{U = C/[R(}n\mathbf{Z^+)(}m\mathbf{Z^-)]} \quad (2)$$

C = constant, crystal structure dependent,
R = cation, anion distance,
$\mathbf{Z^+}$, $\mathbf{Z^-}$ = cation, anion charge,
n, m = number of cations, anions.

For a 1:1 salt such as CsI, n, m, $\mathbf{Z^+}$, and $\mathbf{Z^-}$ = 1, then C/R is equal to U which in this case is −144 Kcal/mole. The value of C/R that is necessary to neutralize the unfavorable energy of the $NdCl_6^{-3}$ anion can be calculated (C/R [(3)(+1)(1)(−3)] = 116) as C/R = −12.9 Kcal/mole. This value is very small. Thus, any cation should produce enough lattice energy to stabilize the $LnCl_6^{-3}$. This is evidenced by the structures reported in the CSD, where a number of $LnCl_6^{-3}$ anions with three monovalent cations are available. Furthermore, double salts, where the additional ions increase the lattice energy, countering the instability of the $LnCl_6$ anions ($[Me_2NH_2]_4[LnCl_6]Cl$ (Ln = Ho, Er, Tm [14]; Ln = Nd, Sm, Eu [15]) and $[MeNH_3]_4[YbCl_6]Cl$) [16,17] have also been reported. Further examples reveal cations with higher charges, such as was noted for [Nd(dimethylurea)$_6$NdCl$_6$][18] or even more complex arrays such as $[MeNH_3]_8[NdCl_6][NdCl_4(H_2O)_2]_2Cl_3$, [19] $[Me_3PyH]_{10}[ErCl_6][ErCl_5(H_2O)]Cl_3$ [20] and $[Nd(EO_4)_2]_4[NdCl_6]Cl_9$ (where EO_4 = tetraethylene glycol) [21].

The C/R term contains two variables: (i) R, which is the distance between the anion and cation and (ii) the Madelung constant, which depends on the detailed arrangement of anions and cations in the lattice. Since R does not vary much between the **Ln-6** and **Ln-5** structures, it will have minimal impact on the final lattice energy. The Madelung constants for several organic salts [22] have been reported to span a small range from 1.16 to 2.52. Since the structures of both **Ln-6** and **Ln-5** are basically a shell of py-H cations

surrounding a Ln-Cl complex, the Madelung constants for the **Ln-6** and **Ln-5** structures are also expected to be very similar and, to enable investigation, were assumed to be identical. Therefore, the lattice energy difference is defined by the $(nZ^+)(mZ^-)$ term, which becomes 9 for **Ln-6** and 4 for **Ln-5**. At the structural switchover, the stability advantage of **Tb-5** (−283 Kcal/mol) over **Gd-6** (+88 Kcal/mol), including the binding energy of the complex anion and H-bonding is calculated to be −371 Kcal/mole (see Table S6). Substituting for the lattice energies of **Ln-6** and **Ln-5**, the equation becomes C/R(9) = C/R(4) −371 Kcal/mol, which solves to C/R = −74 Kcal/mole. Lattice energies larger than this value will favor the **Ln-6** structure over the **Ln-5** arrangement. Recalling that the lattice energy for CsI is −144 Kcal/mole, −74 Kcal/mole is a very small lattice energy. Therefore, the **Ln-5** structure can exist only if the lattice energy is small. This conclusion was based on the assumption that the C/R term for the **Ln-6** and **Ln-5** structures are the same, which is not true. However, the range of Madelung constants is small, so even if a generous 50% difference exists between the two C/R terms, the lattice energy required for the **Ln-6** structure to dominate [−74 + 0.5(−74) Kcal/mol = −111 Kcal/mol], remains small.

Crystal Stress Analysis

The shortest contacts between a cationic N and a Cl ligand are listed in Table S1. As the series is traversed the metal radii shrinks which results in a decrease in the N●●●Cl contacts, resulting in slightly larger lattice energies for both the Ln-6 and Ln-5 structures. For the **Ln-6** structures, nearly all contacts stay constant or decrease slightly from La to Gd. There is, however, an anomaly as the N(70)---Cl(24) and N(70)---Cl(26) distances increase between Eu and Gd. This suggests a stress is building in the **Ln-6** structure, which is relieved after Gd due to the **Ln-5** structure transition. In the **Ln-6** structures there are four repulsive contacts between cations and all of these involve the py-H-py cation. (See Table S3). Three of these cation–cation distances are between 3.6 and 3.8 Å and do not change across the series; however, for the fourth contact, the decrease from La (3.66 Å) to Pr (3.49 Å) to Gd (3.46 Å) results in an increasingly destabilized **Ln-6** structure. There are no such short cation–cation contacts in the **Ln-5** structure. As noted previously, the complex Cl anions in all three structures are surrounded by a shell of py-H and/or py-H-py cations. As the Ln ions become smaller, the anions shrink until there is no space in the surrounding cation layer for one of the pyridine rings. At that point the py-H-py cation is lost, tipping the stability to the **Ln-5** structure. Based upon the structures observed, this change occurs between Gd and Tb.

Stress Summary

From these evaluations, it is apparent that the overall energy variation between **Ln-6** and **Ln-5** is very small. The **Ln-6** structure is favored based on the lattice energy and H-bonding, whereas **Ln-5** is favored only by the greater binding energy of the $LnCl_5(py)^{-2}$ anion. In order for the **Ln-6** and **Ln-5** structures to co-exist, the C/R value has been estimated to be the small value of −74 Kcal/mole (*vide supra)*. Thus, the **Ln-5** structure can only exist when the lattice energy is small.

3. Materials and Methods

All complexes described below were handled under an atmosphere of argon with rigorous exclusion of air and water using standard Schlenk line and glove box techniques unless otherwise stated. The **$[Ln(H_2O)_n(Cl)_3]$** precursors were either purchased (Sigma-Aldrich Chemical Company) or synthesized and crystallographically verified from Ln(0) or Ln_2O_3 in concentrated HCl. Pyridine (99.99% anhydrous) was used as received (Sigma-Aldrich).

3.1. Ln-6 General Synthesis

In an argon filled glovebox, **$[Ln(H_2O)_n(Cl)_3]$** (1.0 g; Ln = Ce, Pr, Nd, Sm, Eu, and Gd) was mixed with pyridine (~10 mL) and stirred overnight. The resulting white slurry was heated to boiling, filtered hot through a glass frit, and the clear mother liquor allowed to

slowly cool to glovebox temperature. Crystals typically grew overnight and were used for all analyses. Yields were not optimized.

[[py-H-py][py-H]$_2$[LaCl$_6$]] (La-6). Used [La(m-Cl)(H$_2$O)$_7$]$_2$•4Cl (1.0 g, 2.8 mmol). FTIR (KBr, cm^{-1}) 3772.96(w), 3695.98(w), 3491(w), 3234.92(w), 3165.27(w), 3065.51(w), 2858.12(w), 2247.39(w), 2030.86(w), 1903.07(w), 1635.05(s), 1610.81(s), 1537.41(s), 1482.62(s), 1384.56(m), 1330.47(m), 1239.42(m), 1196.64(m), 1163.31(m), 1078.45(w), 1045.24(m), 1027.68(m), 883.5(m), 800.42(w), 742.43(s), 674.6(s), 608.56(m), 466.31(w).

[[py-H-py][py-H]$_2$[CeCl$_6$]] (Ce-6). Used [Ce(m-Cl)(H$_2$O)$_7$]$_2$•4Cl (1.0 g, 2.8 mmol). FTIR (KBr, cm^{-1}) 3774.08(w), 3696.98(w), 3640.17(w), 3388.9(m), 3225.73(m), 3160.73(m), 3062.61(m), 2960.36(m), 2859.76(m), 2431.3(m), 2010.37(m), 1725.23(w), 1709.64(w), 1632.98(s), 1610.05(s), 1530.13(s), 1484.03(s), 1445.41(m), 1407.12(m), 1332.49(m), 1248.52(m), 1196.69(m), 1164.75(m), 1039.43(m), 1006.05(m), 895.41(m), 803.22(w), 747.48(s), 677.03(s), 630.23(m), 608.69(m), 572.35(m), 516.64(m), 503.25(m), 489.23(m), 476.23(m), 464.99(m), 432.34(w).

[[py-H-py][py-H]$_2$[PrCl$_6$]] (Pr-6). Used [Pr(m-Cl)(H$_2$O)$_7$]$_2$•4Cl (1.0 g, 2.8 mmol). 3910.89(w), 3860.01(w), 3845.5(w), 3027.46(w), 3774.15(w), 3696.91(w), 3682.41(w), 3661.92(w), 3638.78(w), 3230.83(m), 3162.37(m), 3066.82(m), 2958.45(m), 2918.67(m), 1902.17(m), 1725.39(w), 1709.57(w), 1690.34(w), 1660.5(w), 1634.75(s), 1610.53(s), 1524.72(s), 1482.39(s), 1447.93(w), 1408.65(w), 1384.25(w), 1330.01(m), 1238.96(m), 1196.07(m), 1163.44(m), 1045.53(m), 1027.31(m), 881.46(m), 802.8(m), 741.4(s), 672.87(s), 608.65(m), 477.2(m), 462.71(m).

[[py-H-py][py-H]$_2$[NdCl$_6$]] (Nd-6). Used [NdCl$_2$(H$_2$O)$_6$]•Cl (1.0 g, 2.7 mmol). FTIR (KBr, cm^{-1}) 3773.75(w), 3696.26(w), 3661.34(w), 3487.35(w), 3230.64(m), 3163.07(m), 3066.45(m), 2958.88(w), 2876.61(m), 2385.43(w), 2247.28(w), 2031.26(m), 1857.95(m), 1725.2(w), 1690.23(w), 1634.91(s), 1610.21(s), 1524.15(s), 1482.68(s), 1386.38(m), 1329.89(m), 1237.87(m), 1196.17(m), 1163.32(m), 1046.5(m), 1027.85(m), 874.62(m), 802.67(m), 763.56(m), 741.07(s), 672.82(s), 608.78(m), 481.28(m), 465.46(m), 452.45(m).

[[py-H-py][py-H]$_2$[SmCl$_6$]] (Sm-6). Used [SmCl$_2$(H$_2$O)$_6$]•Cl (1.0 g, 2.7 mmol). FTIR (KBr, cm^{-1}) 3768.91(w), 3696.9(w), 3489.46(w), 3257.29(m), 3068.2(w), 2851.65(w), 2438.27(w), 2245.76(w), 2004.26(m), 1861.29(m), 1690.42(w), 1635.38(s), 1610.82(s), 1535.49(s), 1483.38(s), 1385.18(m), 1329.81(s), 1240.08(s), 1195.9(s), 1162.83(s), 1047.83(s), 1027.69(s), 990.16(s), 879.18(s), 743.46(s), 670.09(s), 608.73(s), 477.95(w), 462.07(w).

[[py-H-py][py-H]$_2$[EuCl$_6$]] (Eu-6). Used [EuCl$_2$(H$_2$O)$_6$]•Cl (1.0 g, 2.7 mmol). FTIR (KBr, cm^{-1}) 3846.12(w), 3772.94(w), 3696.39(w), 3662.6(w), 3639.83(w), 3471.14(w), 3234.01(m), 3169.04(m), 3070.65(m), 2898.95(m), 2594.46(w), 2469.78(m), 2348.75(w), 2244.3(m), 2005.72(m), 1969.08(m), 1857.52(m), 1726.58(m), 1709.94(w), 1690.94(m), 1660.11(m), 1634.52(s), 1610.52(s), 1534.22(s), 1484.72(s), 1444.93(s), 1404.77(m), 1385(m), 1325.69(m), 1236.86(m), 1221.76(s), 1196.81(s), 1163.36(s), 1063.65(s), 1039.57(s), 1027.82(s), 1006.78(s), 980.52(m), 870.47(s), 807.83(w), 763.36(s), 740.45(s), 710.9(m), 671.49(s), 625.68(m), 608.96(m), 477.88(w), 464(w), 441.05(s).

[[py-H-py][py-H]$_2$[GdCl$_6$]] (Gd-6). Used [GdCl$_2$(H$_2$O)$_6$]•Cl (1.0 g, 2.7 mmol). FTIR (KBr, cm^{-1}) 3965(w), 3765.31(w), 3693.93(w), 3432.15(w), 3255.08(w), 2851.21(w), 2647.12(w), 2594.53(w), 2469.36(w), 2244.28(w), 2006.43(m), 1967.82(m), 1858(m), 1727.55(w), 1690.39(w), 1635.32(s), 1611.06(s), 1574.51(m), 1534.76(s), 1485.87(s), 1444.45(s), 1404.79(m), 1384.71(m), 1325.22(s), 1236.66(m), 1222.16(s), 1196.74(s), 1163.04(s), 1081.02(m), 1064.56(s), 1040.55(s), 1008.45(m), 979.04(s), 927.64(w), 869.32(s), 806.16(m), 762.97(s), 709.47(m), 670.24(m), 626.94(s), 608.71(m), 480.92(m), 426.02(s).

3.2. Ln-5 General Syntheses

In a glovebox under argon, **[Ln(H$_2$O)$_n$(Cl)$_3$]** (1.0 g; Ln = Tb, Dy, Ho, Er, Tm, Yb, and Lu) was mixed with pyridine (~10 mL) and stirred overnight. The resulting clear solution was heated to a boil, which resulted in a slurry. The reaction mixture was filtered hot and upon cooling, X-ray quality crystals were isolated. Yields were not optimized.

[[py-H]$_2$[TbCl$_5$(py)]] (Tb-5). Used [TbCl$_2$(H$_2$O)$_6$]•Cl (1.0 g, 2.7 mmol). FTIR (KBr, cm^{-1}) 3684.54(w), 3232.2(m), 3171.03(m), 3103.73(m), 3066.41(m), 3037.55(m), 2997.84(m), 2923.11(m), 2637.73(w), 2601.67(w), 2461.5(w), 2378.31(w), 2306.69(w), 2221.59(w), 2005.99(m),

1932.71(m), 1876.56(m), 1771.47(w), 1710.68(w), 1633.71(s), 1599.96(s), 1535.09(m), 1487.84(s), 1443.18(s), 1388.06(m), 1365.53(m), 1325.19(m), 1222.3(s), 1198.45(m), 1153.67(s), 1071.68(s), 1037.26(s), 1005.41(s), 870.42(m), 758.26(s), 698.16(s), 673.61(s), 623.03(s), 475.44(w).

[[py-H]$_2$[DyCl$_5$(py)]] (Dy-5). Used [DyCl$_2$(H$_2$O)$_6$]•Cl (1.0 g, 2.7 mmol). FTIR (KBr, cm^{-1}) 3457.31(w), 3233.87(w), 3172.64(w), 3069.04(w), 2997.42(w), 2923.04(w), 2461.51(w), 2306.36(w), 2005.84(m), 1933.22(m), 1875.68(m), 1635.09(s), 1600.9(s), 1533.44(s), 1487.41(s), 1443.96(s), 1386.96(m), 1325.73(m), 1222.58(s), 1198.56(m), 1153.48(s), 1070.31(s), 1037.99(s), 1006.31(s), 870.74(m), 758.4(s), 701.5(s), 674.32(s), 624.16(s), 532.06(w), 477.56(w).

[[py-H]$_2$[HoCl$_5$(py)]] (Ho-5). Used [HoCl$_2$(H$_2$O)$_6$]•Cl (1.0 g, 2.6 mmol). FTIR (KBr, cm^{-1}) 3684.47(w), 3233.83(w), 3183(w), 3070.02(w), 2922.56(w), 2638.54(w), 2461.47(w), 2380.21(w), 2306.64(w), 2006.69(w), 1933.86(w), 1875.23(m), 1776.36(w), 1711.28(w), 1690.31(w), 1634.4(s), 1600.45(s), 1534.57(s), 1487.51(s), 1442.53(s), 1387.02(m), 1366.62(m), 1324.9(m), 1222.89(s), 1197.84(s), 1154.64(s), 1071.29(s), 1037.65(s), 1005.86(s), 869.48(s), 762.16(s), 672.64(m), 623.34(m).

[[py-H]$_2$[ErCl$_5$(py)]] (Er-5). Used [ErCl$_2$(H$_2$O)$_6$]•Cl (1.0 g, 2.6 mmol). FTIR (KBr, cm^{-1}) 3233.22(w), 3066.09(w), 2998.2(w), 2923.08(w), 2460.91(w), 2306.48(w), 2004.86(m), 1934.58(m), 1876.39(m), 1711.38(w), 1634.6(s), 1600.46(s), 1534.97(s), 1487.79(s), 1442.82(s), 1388.13(m), 1365.46(m), 1325.4(m), 1223.11(s), 1198.74(m), 1153.95(s), 1071.44(s), 1037.89(s), 1006.09(s), 949.9(w), 880.65(m), 758.62(s), 707.06(s), 623.45(s), 499.35(w), 466.09(w).

[[py-H]$_2$[TmCl$_5$(py)]] (Tm-5). Used [TmCl$_2$(H$_2$O)$_6$]•Cl (1.0 g, 2.6 mmol). FTIR (KBr, cm^{-1}) 3454.91(w), 3233.43(m), 3172.46(m), 3104.34(m), 3070.69(m), 2997.9(w), 2962.49(w), 2922.94(m), 2461.36(m), 2224.92(w), 2006.04(m), 1874.5(m), 1710.29(w), 1635.65(s), 1601.84(s), 1535.29(s), 1487.26(s), 1444.61(s), 1387.05(m), 1325.53(m), 1223.15(s), 1198.49(m), 1154.7(m), 1070.93(s), 1038.83(s), 1006.54(s), 871.43(m), 757.97(s), 699.9(s), 674.09(s), 625.04(s), 476,7(w).

[[py-H]$_2$[YbCl$_5$(py)]] (Yb-5). Used [YbCl$_2$(H$_2$O)$_6$]•Cl (1.0 g, 2.6 mmol). FTIR (KBr, cm^{-1}) 3468.16(w), 3233.69(w), 3172.85(w), 3070.81(m), 2923.74(w), 2009.28(w), 1864.61(w), 1636.39(s), 1602.99(s), 1535.4(s), 1486.5(s), 1444.66(s), 1325.91(m), 1222.14(s), 1198.56(m), 1163.6(m), 1066.91(s), 1039.86(s), 1007.38(s), 872.12(m), 741.21(s), 700.86(s), 674.28(s), 628.17(s), 577.87(m).

[[py-H]$_2$[LuCl$_5$(py)]] (Lu-5). Used [LuCl$_2$(H$_2$O)$_6$]•Cl (1.0 g, 2.6 mmol). FTIR (KBr, cm^{-1}) 3233.9(w), 2923.47(w), 2007.68(m), 1859.56(m), 1636.09(s), 1610.98(s), 1534.48(s), 1485.69(s), 1445.22(s), 1405.95(w), 1385.32(m), 1324.82(s), 1224.47(s), 1197.48(s), 1163.6(s), 1065.22(s), 1041.57(s), 1028.73(s), 1008.19(s), 980.85(s), 870.5(s), 765.75(s), 740.12(s), 710.89(m), 672.71(s), 627.69(s), 608.66(m), 452.65(w).

4. Analytical Analyses

All samples used for analytical analyses were dried and handled under an argon atmosphere.

4.1. Infrared Spectroscopy

All samples were prepared under an argon atmosphere using a hand press. FT-IR spectroscopic data were collected on a Nicolet 6700 FT-IR spectrometer using a KBr pellet press under a flowing atmosphere of nitrogen.

4.2. X-ray Crystal Structure Information

For each sample, single crystals were mounted onto a loop from a pool of Fluorolube™ (Sigma-Aldrich, MO, USA) or Parabar 10312 (Hampton Research, Aliso Viejo, CA, USA) and immediately placed in a 100 K N_2 vapor stream. X-ray intensities were measured using a Bruker APEX-II CCD diffractometer with MoKα radiation (λ = 0.71070 Å). Indexing, frame integration, and structure solutions were performed using the Bruker SHELXTL [23–25] software package within the Apex3 [23] and/or OLEX2 [26] suite of software. Additional information concerning the data collection and final structural solutions can be found by accessing CIF files through the Cambridge Crystallographic Database [10]. The unit cell

parameters for all compounds are available in Table 1 and select metrical data available in Table 2. Specific details of the structure solution are discussed below.

The previous reports concerning the [[py-H]$_2$[LnCl$_5$(py)] (Ln = Eu, Er, Yb) [8] structures were solved in the Pnma space group. With our data in the Pnma model, the PyH cation was rotationally disordered by about 10 degrees in a 1:1 ratio for all of the **Ln-5** compounds. Additionally, for all the **Ln-5** compounds, the R value for the intrinsic phasing solution for the noncentric space group Pna2$_1$ was about half that of the Pnma models. The final R values for the Pna2$_1$ solutions were less than 2.3% in all cases, see Table 1. The results of a statistical significance F-test [27] are presented in Table S7 in the supporting information and these data clearly indicate, in all cases, that the Pna2$_1$ model is favored at much more than the 99% confidence level. The descriptions of the two structures solutions are very similar; in each case the py-H cation resides between two [LnCl$_5$p(py)] anions and forms a bifurcated N-H●●●Cl bond. The previously reported Pnma structure for the Er derivative [8] possesses two py-H cations that are symmetry related by a mirror plane. This results in two mirror related N atoms, separated by 5.062 Å, H-bonding to the same pair of Cl ligands [Cl(1) and Cl(2) in our numbering system]. For the Pna2$_1$ structure in this study, the two py-H cations are not equivalent. The N(20) atom H bonds to Cl(1) and Cl(2) as in the Pnma description, but the N(30) atom H bonds to Cl(2) and Cl(4). This results in a longer distance between the N atoms at 5.122 Å. The Pna21 crystals are racemically twinned with ratios between 0.350(8) and 0.500(9).

5. Summary and Conclusions

Attempts to dehydrate **[Ln(H$_2$O)$_n$(Cl)$_3$]** using pyridine led to the isolation of two types of polychloride Ln-species, crystallographicaly characterized as [[py-H-py][py-H]$_2$[LnCl$_6$]] (**Ln-6**; Ln = La, Ce, Pr, Nd, Sm, Eu, Gd) or [[py-H]$_2$[LnCl$_5$(py)]] ((**Ln-5**; Ln = Tb, Dy, Ho, Er, Tm, Yb, Lu). Extensive H-bonding, between the py-H cations and the Ln-anions stabilizes the crystal. The addition of the py bonding energy appears to favor the **Ln-5** structures, whereas the introduction of the py-H-py cation adds enough lattice energy to favor the **Ln-6**. The structure change from **Ln-6** to **Ln-5**, is believed to occur due to the decreasing size of the Ln cation eliminating the space necessary for the py-H-py stabilizing counter cation. Thus, Coulombic energy, H-bonding and the Ln-contraction combine to dictate the final structural arrangements observed herein. It is apparent that this 'simple' system of **[Ln(H$_2$O)$_n$(Cl)$_3$]** and pyridine is much more complex than anticipated.

Supplementary Materials: The following supporting information can be downloaded at: https://www.mdpi.com/article/10.3390/molecules28010283/s1, Figure S1: Analytical FTIR data for **[LaCl$_6$]●py-H-py**, **2(H-py) (La-6)**, Figure S2: Analytical FTIR data for **[CeCl$_6$]●py-H-py**, **2(H-py) (Ce-6)**, Figure S3: Analytical FTIR data for **[NdCl$_6$]●py-H-py**, **2(H-py) (Nd-6)**, Figure S4: Analytical FTIR data for **[SmCl$_6$]●py-H-py**, **2(H-py) (Sm-6)**, Figure S5: Analytical FTIR data for **[EuCl$_6$]●py-H-py**, **2(H-py) (Eu-6)**, Figure S6: Analytical FTIR data for **[GdCl$_6$]●py-H-py**, **2(H-py) (Gd-6),** Figure S7: Analytical FTIR data for **[TbCl$_5$(py)]●2(H-py) (Tb-5)**, Figure S8: Analytical FTIR data for **[DyCl$_5$(py)]●2(H-py) (Dy-5)**, Figure S9: Analytical FTIR data for **[HoCl$_5$(py)]●2(H-py) (Ho-5)**, Figure S10: Analytical FTIR data for **[ErCl$_5$(py)]●2(H-py) (Er-5)**, Figure S11: Analytical FTIR data for **[TmCl$_5$(py)]●2(H-py) (Tm-5)**, Figure S12: Analytical FTIR data for **[YbCl$_5$(py)]●2(H-py) (Yb-5)**, Figure S13: Analytical FTIR data for **[LuCl$_5$(py)]●2(H-py) (Lu-5)**, Figure S14: Analytical FTIR data for **[PrCl$_6$]●py-H-py, 2(H-py) (Pr-6)**, Figure S15: Theoretical PXRD data for **[LaCl$_6$]●py-H-py**, **2(H-py) (La-6)**, Figure S15.1: Experimental PXRD data for **[LaCl$_6$]●py-H-py**, **2(H-py) (La-6)**, Figure S16: Theoretical PXRD data for **[CeCl$_6$]●py-H-py**, **2(H-py) (Ce-6)**, Figure S16.1: Experimental PXRD data for **[CeCl$_6$]●py-H-py**, **2(H-py) (Ce-6)**, Figure S17: Theoretical PXRD data for **[NdCl$_6$]●py-H-py**, **2(H-py) (Nd-6)**, Figure S17.1: Experimental PXRD data for **[NdCl$_6$]●py-H-py**, **2(H-py) (Nd-6)**, Figure S18: Theoretical PXRD data for **[SmCl$_6$]●py-H-py**, **2(H-py) (Sm-6)**, Figure S18.1: Experimental PXRD data for **[SmCl$_6$]●py-H-py**, **2(H-py) (Sm-6)**, Figure S19: Theoretical PXRD data for **[EuCl$_6$]●py-H-py**, **2(H-py) (Eu-6)**, Figure S19.1: Experimental PXRD data for **[EuCl$_6$]●py-H-py**, **2(H-py) (Eu-6)**, Figure S20: Theoretical PXRD data for **[GdCl$_6$]●py-H-py, 2(H-py) (Gd-6)**, Figure S20.1: Experimental PXRD data for **[GdCl$_6$]●py-H-py, 2(H-py) (Gd-6),** Figure S21: Theoretical PXRD

data for **[$TbCl_5$(py)]●2(H-py) (Tb-5)**, Figure S21.1: Experimental PXRD data for **[$TbCl_5$(py)]●2(H-py) (Tb-5)**, Figure S22: Theoretical PXRD data for **[$DyCl_5$(py)]●2(H-py) (Dy-5)**, Figure S22.1: Experimental PXRD data for **[$DyCl_5$(py)]●2(H-py) (Dy-5)**, Figure S23: Theoretical PXRD data for **[$HoCl_5$(py)]●2(H-py) (Ho-5)**, Figure S23.1: Experimental PXRD data for **[$HoCl_5$(py)]●2(H-py) (Ho-5)**, Figure S24: Theoretical PXRD data for **[$ErCl_5$(py)]●2(H-py) (Er-5)**, Figure S24.1: Experimental PXRD data for **[$ErCl_5$(py)]●2(H-py) (Er-5),** Figure S25: Theoretical PXRD data for **[$TmCl_5$(py)]●2(H-py) (Tm-5),** Figure S25.1: Experimental PXRD data for **[$TmCl_5$(py)]●2(H-py) (Tm-5),** Figure S26: Theoretical PXRD data for **[$YbCl_5$(py)]●2(H-py) (Yb-5),** Figure S26.1: Experimental PXRD data for **[$YbCl_5$(py)]●2(H-py) (Yb-5),** Figure S27: Theoretical PXRD data for **[$LuCl_5$(py)]●2(H-py) (Lu-5)**, Figure S27.1: Experimental PXRD data for **[$LuCl_5$(py)]●2(H-py) (Lu-5)**, Figure S28: Theoretical PXRD data for **[$PrCl_6$]●py-H-py, 2(H-py) (Pr-6)**, Figure S28.1: Experimental PXRD data for **[$PrCl_6$]●py-H-py**, **2(H-py) (Pr-6)**; Table S1: Metrical data for **Ln-6**. All distances are in Å, Table S2: Metrical data for **Ln-5**. All distances are in Å, Table S3: Cation–cation contacts in **Ln-6** structures, Table S4: C-H●●●Cl hydrogen bonds in the **Ln-5** structures, Table S5: C-H●●●Cl Hydrogen bonds in the **Pr-6** structure, Table S6: Coulombic energies (Kcal/mol) for **Nd-6**, **Gd-6**, **Tb-5**, and **Lu-5**, Table S7: F-test results for Ln-5 species.

Author Contributions: R.E.C.: validation, formal analysis, investigation, data curation, writing—original draft preparation, writing—review and editing, visualization. E.M.B.: methodology, validation, investigation, data curation. T.J.B.: conceptualization, methodology, validation, formal analysis, investigation, resources, data curation, writing—original draft preparation, writing—review and editing, visualization, supervision, project administration, funding acquisition. All authors have read and agreed to the published version of the manuscript.

Funding: This work was supported was supported in part by the Consortium of Hybrid and Resilient Energy Systems (CHRES), which is sponsored by the NNSA Minority Serving Institutes Partnership Program (MSIPP). Sandia is a multi-mission laboratory managed and operated by National Technology and Engineering Solutions of Sandia, LLC., a wholly owned subsidiary of Honeywell International, Inc., for the U.S. Department of Energy's National Nuclear Security Administration under contract DE-NA-0003525. This paper describes objective technical results and analysis. Any subjective views or opinions that might be expressed in the paper do not necessarily represent the views of the U.S. Department of Energy or the United States Government.

Data Availability Statement: CCDC 2214067–2214080 contains the supplementary crystallographic data for 1–8. These data can be obtained free of charge via from the Cambridge Crystallographic Data Centre, 12 Union Road, Cambridge CB2 1EZ, UK; fax: (+44) 1223-336-033; or e-mail: deposit@ccdc.cam.ac.uk.

Conflicts of Interest: The authors declare no conflict of interest.

References

1. Boyle, T.J.; Guerrero, F.; Cramer, R.E.; Boye, D.A.; Brooks, H.; Reuel, P.C. Synthesis and Characterization of Solvated Lanthanide Tris(trimethylsilyl)siloxides. *Inorg. Chem.* **2022**, *61*, 5048–5059. [CrossRef] [PubMed]
2. *Lanthanides Isolation and Production*; Web Solutions, LLC.: Waukesha, WI, USA, 2022. Available online: https://science.jrank.org/pages/3825/Lanthanides-Isolation-production.html (accessed on 20 September 2022).
3. Boyle, T.J.; Ottley, L.A.M. Lanthanide halides. In *The Rare Earth Elements: Fundamentals and Applications*; Atwood, D., Ed.; Wiley & Sons Ltd.: Hoboken, NJ, USA, 2012.
4. Gruber, V.; Carsky, M. New technology for lanthanide recovery from spent Nd-Fe-B magnets. *S. Afr. J. Chem. Eng.* **2020**, *33*, 35–38. [CrossRef]
5. Mitchem, S. Scientists Gain Insight into Recycling Processes for Nuclear and Electronic Waste. Argonne National Laboratory, 2012. Available online: https://www.anl.gov/article/scientists-gain-insight-into-recycling-processes-for-nuclear-and-electronic-waste (accessed on 20 September 2022).
6. Taylor, M.D. Preparation of Anhydrous Lanthanon Halides. *Chem. Rev.* **1962**, *62*, 503–511. [CrossRef]
7. Boyle, T.J.; Cramer, R.E.; Fasulo, F.; Padilla, N. Solvation coordination compounds of scandium chloride from the dehydration of scandium chloride hexahydrate. *Polyhedron* **2021**, *208*, 115437. [CrossRef]
8. Li, J.-S.; Neumuller, B.; Dehnicke, K. Pyridinium-Chlorometallate von Lanthanoid-Elementen. Die Kristallstrukturen von $[HPy]_2[LnCl_5(Py)]$ mit Ln = Eu, Er, Yb und von $[H(Py)_2][YbCl_4(Py)_2] \cdot Py$. *Z. Anorg. Allg. Chem.* **2002**, *628*, 2785–2789. [CrossRef]
9. Cook, D. Vibrational Spectra of pyridinium salts. *Can. J. Chem.* **1961**, *39*, 2009–2024. [CrossRef]
10. Groom, C.R.; Bruno, I.J.; Lightfoot, M.P.; Ward, S.C. The Cambridge Structural Database. *Acta Crystallogr. Sec. E* **2016**, *B72*, 171–179. [CrossRef]

11. Cramer, R.E.; Rimsza, J.M.; Boyle, T.J. Lanthanide Contraction is a variable. *Inorg. Chem.* **2021**, *61*, 6120–6127. [CrossRef]
12. Szalewicz, K. *Hydrogen Bond Encyclopedia of Physical Science and Technology*, 3rd ed.; Academic Press: Cambridge, MA, USA, 2003; pp. 505–538.
13. Löble, M.W.; Keith, J.M.; Altman, A.B.; Stieber, S.C.E.; Batista, E.R.; Boland, K.S.; Conradson, S.D.; Clark, D.L.; Pacheco, J.L.; Kozimor, S.A.; et al. Covalency in Lanthanides. An X-ray Absorption Spectroscopy and Density Functional Theory Study of $LnCl_6^{x-}$ (x = 3, 2). *J. Am. Chem. Soc.* **2015**, *137*, 2506–2523. [CrossRef]
14. Becker, A.; Urland, W. Crystal structures and magnetic behaviour of new complex lanthanide chlorides with organic cations. *J. Alloys Compd.* **1998**, *24*, 62–66. [CrossRef]
15. Petricek, S. Syntheses and Crystal Structures of Anionic Lanthanide Chloride Complexes $[(CH_3)_2NH_2][LnCl_4(HMPA)_2]$ (Ln = La, Nd) and $[(CH_3)_2NH_2]_4[LnCl_6]Cl$ (Ln = Nd, Sm, Eu). *Acta Chim. Slov.* **2005**, *52*, 398–403.
16. Czjek, M.; Fuess, H. Crystal structure of tetra(monomethylammonium) hexachloroytterbatochloride $(CH_3NH_3)4YbCl_7$. *Z. Krist. Cryst. Mater.* **1987**, *179*, 49.
17. Czjek, M.; Fuess, H.; Pabst, I. Crystal structure and magnetic properties of tetra(monomethylammonium) hexachloroytterbatochloride ($CH_3NH_3)_4YbCl_7$. *Z. Anorg. Allg. Chem.* **1992**, *617*, 105–109. [CrossRef]
18. Diamantopoulou, E.; Papefstathiou, G.S.; Terzis, A.; PRaptopoulou, C.P.; Desseyn, H.O.; Perlepes, S.P. Hydrogen bonded networks based on lanthanide(III) complexes of N,N′-dimethylurea (DMU): Preparation, characterisation, and crystal structures of [Nd(DMU)(6)][$NdCl_6$] and [Nd(NO_3)(3)(DMU)(3)]. *Polyhedron* **2003**, *22*, 825. [CrossRef]
19. Runge, P.; Shulze, M.; Urland, W. Darstellung und Kristallstruktur von $(CH_3NH_3)_8[NdCl_6][NdCl_4(H_2O)_2]_2Cl_3$. *Z. Anorg. Allg. Chem.* **1991**, *592*, 115–120. [CrossRef]
20. Hallfeldt, J.; Urland, W. Synthese, Kristallstruktur und magnetisches Verhalten von (2,4,6-Trimethylpyridinium)–$[ErCl_6][ErCl_5(H_2O)]_2Cl_3$. *Z. Anorg. Allg. Chem.* **2002**, *628*, 2661–2664. [CrossRef]
21. Rogers, R.D.; Rollins, A.N.; Henry, R.F.; Murdoch, J.S.; Etzenhouser, R.D.; Huggins, S.E.; Nunez, L. Direct comparison of the preparation and structural features of crown ether and polyethylene glycol complexes of neodymium trichloride hexahydrate. *Inorg. Chem.* **1991**, *30*, 4945–4954. [CrossRef]
22. Izgorodina, E.I.; Bernard, U.L.; Dean, P.M.; Pringle, J.M.; MacFarlane, D.R. The Madelung Constant of Organic Salts. *Cryst. Growth Des.* **2009**, *11*, 4834–4839. [CrossRef]
23. *The SHELEX Suite of Package of Programs—Saint, SADABS, Apex3*; Bruker AXS: Madison, WI, USA, 2012.
24. Sheldrick, G.M. A short history of SHELX. *Acta Crystallogr. Sect. A* **2008**, *64*, 112–122. [CrossRef]
25. Sheldrick, G.M. Crystal structure refinement with SHELXL. *Acta Crystallogr. Sect. C* **2015**, *C17*, 3–8.
26. Dolomanov, O.V.; Bourhis, L.J.; Gildea, R.J.; Howard, J.A.K.; Pushmann, H. OLEX2: A complete structure solution, refinement and analysis program. *J. Appl. Cryst.* **2009**, *42*, 339–341. [CrossRef]
27. Downward, L.; Booth, C.H.; Lukens, W.W.; Bridges, F. A Variation of the F-Test for Determining Statistical Relevance of Particular Parameters in EXAFS Fits. *AIP Conf. Proc.* **2007**, *882*, 129–131.